

 Open access • Posted Content • DOI:10.1101/705277

## 3D imaging of colorectal cancer organoids identifies responses to Tankyrase inhibitors

— [Source link](#) 

Luned Badder, Andrew John Hollins, Bram Herpers, Kuan Yan ...+14 more authors

**Institutions:** Cardiff University, University Hospital of Wales, Merck & Co.

**Published on:** 18 Jul 2019 - bioRxiv (Cold Spring Harbor Laboratory)

**Topics:** Cancer stem cell, Wnt signaling pathway, Colorectal cancer and Cancer cell

Related papers:





- [182 TRAP1 represents a key mediator of stemness and glycolytic metabolism in colorectal cancer cells](#)
- [The interaction of Wnt-11 and signalling cascades in prostate cancer](#)
- [Canonical and non-canonical WNT signaling in cancer stem cells and their niches: Cellular heterogeneity, omics reprogramming, targeted therapy and tumor plasticity \(Review\)](#)
- [Somatic Tissue Engineering in Mouse Models Reveals an Actionable Role for WNT Pathway Alterations in Prostate Cancer Metastasis.](#)
- [Wnt/ \$\beta\$ -catenin signaling in melanoma: Preclinical rationale and novel therapeutic insights](#)

Share this paper:    

View more about this paper here: <https://typeset.io/papers/3d-imaging-of-colorectal-cancer-organoids-identifies-28ljtd69o9>

## RESEARCH ARTICLE

## 3D imaging of colorectal cancer organoids identifies responses to Tankyrase inhibitors

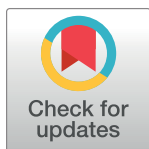
Luned M. Badder<sup>1,2</sup>, Andrew J. Hollins<sup>1,2</sup>, Bram Herpers<sup>3</sup>, Kuan Yan<sup>3</sup>, Kenneth B. Ewan<sup>1</sup>, Mairian Thomas<sup>4</sup>, Jennifer R. Shone<sup>1</sup>, Delyth A. Badder<sup>5</sup>, Marc Naven<sup>6</sup>, Kevin E. Ashelford<sup>6</sup>, Rachel Hargest<sup>7,8</sup>, Alan R. Clarke<sup>2†</sup>, Christina Esdar<sup>9</sup>, Hans-Peter Buchstaller<sup>9</sup>, J. Mark Treherne<sup>4</sup>, Sylvia Boj<sup>10</sup>, Bahar Ramezanzpour<sup>10</sup>, Dirk Wienke<sup>9</sup>, Leo S. Price<sup>3</sup>, Paul H. Shaw<sup>11</sup>, Trevor C. Dale<sup>2\*</sup>

**1** Cardiff University School of Biosciences, Cardiff, Wales, United Kingdom, **2** European Cancer Stem Cell Research Institute (ECSCRI), Cardiff University, Cardiff, Wales, United Kingdom, **3** Ocello B.V., Leiden, The Netherlands, **4** Cellesce Ltd, Cardiff Medicentre, Heath Park, Cardiff, United Kingdom, **5** Cellular Pathology Department, University Hospital for Wales, Cardiff, United Kingdom, **6** Division of Cancer and Genetics, School of Medicine, Cardiff University, Cardiff, United Kingdom, **7** Department of Colorectal Surgery, University Hospital of Wales, Cardiff, United Kingdom, **8** Division of Cancer and Genetics, CCMRC, Henry Wellcome Building, Cardiff University, Cardiff, United Kingdom, **9** Biopharma, Merck Healthcare KGaA, Research & Development, Darmstadt, Germany, **10** Hubrecht Organoid Technology, Utrecht, The Netherlands, **11** Velindre Cancer Centre, Cardiff, Wales, United Kingdom

 These authors contributed equally to this work.

† Deceased.

\* [DaleTC@cardiff.ac.uk](mailto:DaleTC@cardiff.ac.uk)


 OPEN ACCESS

**Citation:** Badder LM, Hollins AJ, Herpers B, Yan K, Ewan KB, Thomas M, et al. (2020) 3D imaging of colorectal cancer organoids identifies responses to Tankyrase inhibitors. *PLoS ONE* 15(8): e0235319. <https://doi.org/10.1371/journal.pone.0235319>

**Editor:** Ning Wei, University of Pittsburgh, UNITED STATES

**Received:** November 1, 2019

**Accepted:** June 12, 2020

**Published:** August 18, 2020

**Copyright:** © 2020 Badder et al. This is an open access article distributed under the terms of the [Creative Commons Attribution License](https://creativecommons.org/licenses/by/4.0/), which permits unrestricted use, distribution, and reproduction in any medium, provided the original author and source are credited.

**Data Availability Statement:** Components within the manuscript (denoted as [S1 Table](#) within the text) are held in a public repository <https://www.ebi.ac.uk/ena/data/view/PRJEB37607> where sequencing information can be found. Other data is all contained within the paper and/or Supporting Information files.

**Funding:** This work was supported by Cancer Research Wales PhD studentship (L.M.B), the Cancer Research UK Cardiff Experimental Cancer Medicine Centres (ECMC) (A.J.H.) and Cancer Research UK Programme Grant C1295/A15937H

## Abstract

Aberrant activation of the Wnt signalling pathway is required for tumour initiation and survival in the majority of colorectal cancers. The development of inhibitors of Wnt signalling has been the focus of multiple drug discovery programs targeting colorectal cancer and other malignancies associated with aberrant pathway activation. However, progression of new clinical entities targeting the Wnt pathway has been slow. One challenge lies with the limited predictive power of 2D cancer cell lines because they fail to fully recapitulate intratumoural phenotypic heterogeneity. In particular, the relationship between 2D cancer cell biology and cancer stem cell function is poorly understood. By contrast, 3D tumour organoids provide a platform in which complex cell-cell interactions can be studied. However, complex 3D models provide a challenging platform for the quantitative analysis of drug responses of therapies that have differential effects on tumour cell subpopulations. Here, we generated tumour organoids from colorectal cancer patients and tested their responses to inhibitors of Tankyrase (TNKSi) which are known to modulate Wnt signalling. Using compounds with 3 orders of magnitude difference in cellular mechanistic potency together with image-based assays, we demonstrate that morphometric analyses can capture subtle alterations in organoid responses to Wnt inhibitors that are consistent with activity against a cancer stem cell subpopulation. Overall our study highlights the value of phenotypic readouts as a quantitative method to assess drug-induced effects in a relevant preclinical model.

<https://www.cancerresearchuk.org> Innovate UK grant 9776 (KE) <https://www.gov.uk/government/organisations/innovate-uk>. The funders did not play any role in study design, data collection and analysis, the decision to publish or the preparation of the manuscript.

**Competing interests:** L.S.P is a founder and major shareholder of Ocello B.V, and C.E., H.-P.B and D.W are employees of Merck Healthcare KGaA. M.T and J.T are employees of Cellesce Ltd. T.C.D is a director of Cellesce Ltd. L.M.B and D.A.B are siblings. The funder provided support in the form of salaries for authors L.S.P, C.E., H.-P.B, D.W, M.T and J.T but did not have any additional role in the study design, data collection and analysis, decision to publish, or preparation of the manuscript. The specific roles of these authors are articulated in the 'author contributions' section. This does not alter our adherence to PLOS ONE policies on sharing data and materials.

**Abbreviations:** CRC, Colorectal cancer; NOD/SCID, Non-obese Diabetic/Severe Combined Immunodeficiency; ODX, Organoid derived xenograft; PARP, poly (ADP-ribose) polymerases; TNKS, Tankyrase.

## Introduction

Aberrant canonical Wnt/ $\beta$ -catenin signalling, as a result of activating mutations within the pathway, has a prominent role in the initiation and progression of colorectal cancer (CRC) [1, 2]. A number of feedback loops control  $\beta$ -catenin turnover and Wnt activation. In the absence of a Wnt ligand the multi-protein  $\beta$ -catenin destruction complex, formed of AXIN1/2, Adenomatous polyposis coli (APC) and glycogen synthase kinase (GSK3 $\beta$ ), mark  $\beta$ -catenin for degradation [3]. As a result, the accumulation and subsequent translocation of  $\beta$ -catenin to the nucleus is inhibited, preventing the downstream activation of target genes [4]. Components of the destruction complex are also tightly regulated. AXIN1 and AXIN2 are concentration-limiting components of the destruction complex. Levels of AXIN1/2 are post-transcriptionally regulated by tankyrases (TNKS1 and TNKS2), members of the poly (ADP-ribose) polymerases (PARP) family of enzymes, which enhance Wnt signalling by targeting AXIN1/2 for degradation [5].

The inhibition of Wnt signalling has been validated as a means of blocking tumour growth in many cancer models [6, 7]. Small molecule inhibitors of TNKS1 and TNKS2 have been shown to reduce Wnt signalling in intestinal cancer cell lines and have been suggested to prevent tumour growth due to their ability to stabilise AXIN1 and AXIN2 levels and as a result, to inhibit  $\beta$ -catenin mediated transcription [5, 8–16]. However, the progression of TNKSi into clinical trials has been restricted due to significant issues of intestinal toxicity within *in vivo* models, emphasising the important role of Wnt signalling in adult tissue homeostasis [17] [18]. Furthermore, the TNKSi described above reduced colorectal cancer cell numbers in 2D culture, but did so with relatively low effect sizes by comparison with their ability to reduce levels of Wnt/TCF-dependent transcription in the same cell lines. Similar partial-efficacy cell line responses were observed during the development of inhibitors of the CDK8 and CDK19 kinases, suggesting that growth in 2D cell culture may not be an optimal readout for compounds that are anticipated to target cancer stem cells [7].

To date, most preclinical *in vitro* studies have relied on the use of conventional 2D cultures of cell lines. Whilst cancer cell lines can be usefully used to study pathway deregulation, they frequently fail to be predictive when used as readouts of anti-tumour efficacy [19]. It is well recognised that immortalised 2D cell lines adapted to growth on plastic poorly represent the intricate cellular cross-talk present in tumours. In particular, they are unable to recapitulate the inter-cellular interactions that form cancer stem cell niches and, as a consequence, such models fail to fully reflect *in vivo* results.

3D tumour organoids have been shown to provide a more complex insight into tumour cell-cell interactions [20, 21] and have been recognised as models with the potential to bridge the gap between *in vitro* and *in vivo* preclinical studies. Organoids that have never been adapted for growth on plastic have been cultured from multiple tumour types, and have been shown to better represent the genetic diversity of distinct tumour subtypes than 2D cell lines [22]. Organoids derived from genetically-engineered mice in which the Wnt pathway had been oncogenically-activated accurately predicted subsequent *in vivo* responses to inhibitors of the CDK8 and CDK19 kinases, while 2D cell culture only showed partial-efficacy [7]. Organoids have been further shown to predict patient responses and might in future be used in the clinic in personalised medicine [23].

The biological and phenotypic complexity of 3D primary organoid cultures allow, in principle, the assessment of compound activity against a subset of inter-cellular signalling that is central to tumour growth. However, most uses of organoid assays to date have relied on fixed end-point metabolic assays (e.g. ATP-level quantification) that aggregates responses in every cell within a population of organoids. To fully exploit the potential of organoid assays, analysis

platforms need to yield quantitative data that can clearly represent compound-induced effects on signalling pathways whose outputs are complex, whilst simultaneously maintaining usability in a high throughput format.

In this work, we generated CRC patient-derived organoids and studied their responses to Tankyrase inhibitors (TNKSi). Using metabolic end point assays, tankyrase inhibition showed partial efficacy, reflecting a limited reduction in the growth of TNKSi-sensitive organoids. Closer examination of organoid responses suggested that TNKSi altered the ratio of stem-like to differentiated cell populations. This subtle effect on the cellular composition of organoids was best reflected by multiparametric imaging analysis of organoids that was nonetheless compatible with high throughput analysis. Our findings demonstrate the potential of a phenotypic approach to assess drug-induced phenotypes in a preclinical setting, which may be applicable to a wider range of therapeutics that target cancer stem cell biology and niches.

## Materials and methods

### Materials

Corning Growth factor-reduced Matrigel was purchased from VWR (#734–1101). Cell culture media were purchased from Invitrogen Life Technologies, and cell culture plastics from Nunc unless otherwise stated. All TNKSi compounds were supplied and synthesized by Merck Healthcare KGaA (Darmstadt, Germany). All stock solutions of compounds were reconstituted in DMSO. Activity of each compound had been assessed prior to shipping using a cell-based immunobead assay to determine TNKSi potency based on the ability of the inhibitors to stabilise the AXIN2 [24]. The determined EC<sub>50</sub> values of 2 nM, 36 nM and 319 nM (Fig 2A) were determined for C1, C2, and C3 respectively.

### Human tissue

Surgically resected patient materials were obtained from University Hospital of Wales by the Wales Cancer Bank with written informed ethical consent from male and female patients (>16 years of age, above the UK age of valid consent) with known or suspected malignant disease and anonymised (WCB project reference #12/001). The Wales Cancer Bank has ethics approval as a Research Tissue Bank from the Wales Research Ethics Committee 3 (reference 16/WA/0256), and is licensed by the Human Tissue Authority under the UK Human Tissue Act (2004) to store human tissue, taken from the living, for research (licence 12107) [25]. These approvals cover the collection of samples (including written consent), processing and storing samples across multiple collection and storage sites. All patient derived material was handled in concordance with HTA regulations. Histological sections of patient tissue were imaged at University Hospital Wales and remained anonymised.

### Organoid culture

The isolation of tumour organoids from patient material was processed as previously described by Sato *et al.*, [20] with some refinements outlined below. Briefly, following surgical resection, tumour samples were obtained and stored in Hibernate A medium (Life Technologies) at 4°C. Tissue pieces were dissected to remove connective tissue and chopped to pieces approximately 2 mm in diameter. Following dissection, carcinoma pieces were washed in PBS then digested enzymatically with Collagenase and Dispase for 30 minutes at 37°C. Once digested, tissue was triturated in PBS at room temperature to release cell fragments from tissue. Cell fragments within the supernatant were then centrifuged for 5 min at 100 rcf, at 4°C. Cell pellets were resuspended in Advanced DMEM/F12 supplemented with 1% GlutaMAX, 1% HEPES buffer

solution and 1% Penicillin/Streptomycin, then filtered (70  $\mu\text{m}$ ). Collected tissue fragments were counted and plated at a density of 1000 cell fragments per 50  $\mu\text{L}$  of Growth Factor Reduced Matrigel (BD Biosciences) in 24 well plates (Nunc). Following Matrigel polymerisation, cells were overlaid with 500  $\mu\text{L}$  of either “7+” or “Full” media and replenished every 4 days. ‘7+’ Media conditions consisted of Advanced DMEM/F12 supplemented with penicillin/streptomycin, 2mM GlutaMAX, 10 mM HEPES, 1 X B27 supplement, 1 X N2 supplement (all Life Technologies), 1 mM N-acetyl-L-cysteine (Sigma-Aldrich). The following additional niche factors were added to generate “Full” media: 50 ng/ml mouse recombinant EGF (Life Technologies), 100 ng/ml mouse recombinant Noggin (Peprotech), 10% RSp0-1 conditioned medium [26], 40% Wnt-3A conditioned medium [20], 500 nM A83-01 (Tocris) and 10  $\mu\text{M}$  SB202190 (Sigma). 10 $\mu\text{M}$  Y-27632 (Tocris) was also added to media for the first three days of culture. Optimal media was determined for each tumour organoid line on the basis of conditions that favoured the most efficient growth of organoids. For subsequent passaging, maintenance in culture and analyses, the most favourable media condition was used. All culture were maintained in humidified incubators at 37°C, 5% CO<sub>2</sub>.

### DNA extraction

DNA extraction from organoid cultures was carried out using a QIAamp DNA Mini Kit (Qiagen) following the manufacturer’s instructions. Purified DNA quality was initially assessed using a Nanodrop1000 (Thermo Fisher). Patient blood samples were processed by the Wales Cancer Bank (WCB), genomic DNA was extracted from 4 ml of whole blood using the ChemicSTAR automated cell lysis and DNA extraction workstation (Hamilton Company) housed within the All Wales Medical Genetics Service (AWMGS) laboratory. Both DNA samples were then passed to the Wales Gene Park for quality control, library preparation and sequencing.

### Whole exome library preparation

The following was carried out by the Wales Gene Park. Genomic DNA was initially quantified using the Qubit® (Life Technologies) and the samples were serially diluted to 5 ng/ $\mu\text{L}$ . 50ng of gDNA was used as the input and the sequencing libraries were prepared using the Illumina® Nextera Rapid Capture Enrichment kit (Illumina Inc.). The steps included fragmentation of gDNA, clean-up of the fragmented DNA, amplification, clean-up of the amplified DNA, hybridisation of probes, capture of the hybridized probes, second hybridization of probes, second capture, clean-up of the captured library, amplification of enriched library, clean-up of the enriched library and finally validation of the complete library. The manufacturer’s instructions were largely followed with extra quantitation steps prior to the hybridization of the probes to ensure that approximately 500 ng of each sample was pooled. The libraries were validated using the Agilent 2100 Bioanalyser and a high-sensitivity kit (Agilent Technologies) to ascertain the insert size, and the Qubit® (Life Technologies) was used to perform the fluorometric quantitation. Following validation, the libraries were normalized to 10 nM, pooled together and clustered on the cBot™2 following the manufacturer’s recommendations. Pools were then sequenced using a 75-base paired-end (2x75bp PE) dual index read format on the Illumina® HiSeq4000 according to the manufacturer’s instructions.

### Whole exome sequencing and mutation calling

Reads were mapped to the human reference genome (GRCh37) with BWA version 0.7.10 [27], and duplicate reads were removed with Samtools version 0.1.19 [28]. Base quality score recalibration was performed using GATK’s BaseRecalibrator (GATK version 4.0.3.0, [29, 30] and GATK’s Mutect2 was used to call somatic variants (tools found at <https://software>).

[broadinstitute.org/gatk/](http://broadinstitute.org/gatk/)). Variants were annotated with Variant Effect Predictor version 91.3 [31], using a cached version of ensemble v91. A custom Perl script was used to extract genes of interest from annotated variant files. Default parameters were used for all software unless otherwise stated. All of the calls reported were cross-checked against the cBioportal database (<https://www.cbioportal.org>) and are those found to have been previously described within the COSMIC database (<https://cancer.sanger.ac.uk/cosmic>) as being “likely oncogenic”.

## Immunohistochemistry

Formalin-fixed paraffin embedded histological sections of patient tissue were processed, imaged and analysed by the Histopathology unit at University Hospital Wales. For organoid histology, organoids embedded within Matrigel were fixed with 4% paraformaldehyde for 15 min at room temperature. Organoids were then lifted from wells and washed several times with PBS prior to embedding within low melting-point agarose, followed by dehydration, paraffin embedding, sectioning and Hematoxylin+Eosin (H&E) staining. Images were acquired on an Olympus Dp26 microscope.

## Western blot detection

Organoids were harvested from 6 X 50  $\mu$ L blobs of Growth factor-reduced Matrigel using Cell Recovery Solution (Corning) for 1 hour on ice. Total protein was extracted from organoids by addition of 500  $\mu$ L of lysis buffer to whole organoids (0.02 M Tris-HCl, 2 mM EDTA, 0.5% v/v NP-40 (IPEGAL) in ddH<sub>2</sub>O containing 1x PhosSTOP phosphatase inhibitor (Roche) and 1x complete Protease Inhibitor Cocktail (Roche)). The lysates were centrifuged at 8000 rcf for 15 min and proteins harvested in the supernatants. Protein content was measured using a BCA protein assay kit (Pierce). Samples were resolved on Novex NuPAGE 4–12% Bis-Tris PAGE gels, and then blotted onto nitrocellulose membranes using the Invitrogen iBlot Dry Blotting cassette system.

Blots were blocked at room temperature for 1 h in 5% w/v milk powder in wash buffer, Tris buffered saline (TBS) plus 0.2% Tween 20. Primary antibodies were diluted in blocking buffer and incubated overnight at 4°C. After washing the blots were incubated with HRP-conjugated secondary antibodies for 1 h at room temperature. Bands were visualized using the enhanced chemoluminescence (SuperSignal West Dura; Pierce). Antibodies and dilutions: TNKS1/2 (Santa Cruz (Tnks1/2 E-10) SC-365897, 1:500), Axin2 (Cell Signalling Technologies 76G6, 1:500) (# 2151),  $\beta$ -actin (Sigma (AC-74) A2228, 1:10,000), anti-mouse or anti-rabbit HRP-conjugated antibodies (GE Healthcare, 1:5000).

## Organoid viability measurements

Organoids in culture were gently dissociated to near-single cell populations using TrypLE (Life Technologies) before resuspension within growth factor-reduced Matrigel, and dispensed into white clear bottomed 96 well plates in 9  $\mu$ L Matrigel per well (400 cells/  $\mu$ L of Matrigel). Following Matrigel polymerization, a 9-point 2-fold dilution range of compounds were diluted in tailored growth medium and dispensed within each well. DMSO was used as a negative control at a final concentration of 0.1%. Following a six day exposure to compounds, Cell Titer Glo 3D (Promega) reagent was applied as per the manufacturer’s guidelines for an endpoint readout. Relative Luminescence values were obtained on a BMG Fluostar plate reader. Dose response curves and EC<sub>50</sub> values were obtained using Microsoft Excel with XLFit plug-in (Version 5.4.0.8).

## High content fluorescence microscopy

Organoid lines previously established in culture were split to single cells using TrypLE (Life Technologies) and seeded within growth factor-reduced Matrigel (Corning) in black clear-bottomed 384 well plates, at 12  $\mu\text{L}$  per well, at a density of 400 cells/ $\mu\text{L}$  Matrigel. Upon polymerisation of Matrigel, growth media containing a titration range of individual compounds or DMSO controls were added to each well prior to incubation at 37°C. Organoids were exposed to compounds for a total of six days prior to fixation in a fix-and stain solution containing 4% para formaldehyde (Sigma Aldrich), 0.2% Triton X-100 (Sigma Aldrich) 0.25 $\mu\text{M}$  rhodamine-phalloidin (Sigma Aldrich) and 1  $\mu\text{g}/\text{ml}$  Hoechst 33258 (Sigma Aldrich) in PBS at 4°C for 24 h. After staining, plates were washed with PBS and sealed. Imaging was performed on an ImageXpress® high-content micro confocal platform (Molecular Devices). A total of 25 Z-stack images were acquired at 10  $\mu\text{m}$  steps through the focal plane per well of a 384 well plate using a 4 X objective. Image stacks were captured from both TRITC channel (EX = 548, EM = 645) and DAPI channel (EX=380, EM = 435) to detect both rhodamine-phalloidin (F-actin) and Hoechst (nuclei).

## High content image analysis

Images obtained using the ImageXpress platform were processed for phenotypic analysis within OMiner™ software (OcellO B.V.) integrated within the KNIME Analytics Platform (Konstanz, Germany, <http://www.knime.org/>) as described previously [32, 33]. Briefly, this software enabled the quantification of z-stack images derived from Hoechst and rhodamine-phalloidin stained organoids. Information from both the DAPI and TRITC channels were used to enhance organoid boundary separation. Masks generated from both channels facilitated the visualisation of main organoid structure, internal morphometries such as individual lumens, as well as nuclei per organoid. Objects that were out of focus were filtered and discarded from analysis. Morphological features were calculated on the basis of individual organoids and pooled for analysis. Multiple features extracted included counts, total area, solidity, and branching of nuclei, lumen and organoid masks.

Feature training between the negative control organoids and the high dose TNKSi treated organoids was performed to condense the phenotypic features and calculate the Euclidian distance. The results are plotted with GraphPad Prism 7 (GraphPad Software, La Jolla, CA). Results are shown as means  $\pm$  standard deviations unless otherwise stated.

## Quantitative real-time PCR

Total RNA was extracted from organoids resuspended in trizol solution (Life Technologies) containing 125  $\mu\text{g}/\text{ml}$  glycogen. cDNA was yielded from purified mRNA using ImProm II Reverse Transcription kit (Promega). Quantitative-RT PCR was then performed using the SensiFAST SYBR Green Hi-ROX master mix (Bioline). Primers were designed (Sigma Aldrich) and listed in [S2 Table](#). All samples were measured in triplicate, with gene expression normalised to GAPDH housekeeping gene. Reactions were measured on a Step One Plus real-time PCR instrument (Applied Biosystems) with relative changes in gene expression calculated using the  $\Delta\Delta\text{Ct}$  method.

## Wholemout immunofluorescent staining

Organoids were seeded as single cells in 96 well plates in 9  $\mu\text{L}$  growth factor reduced Matrigel at a density of 400 cells/ $\mu\text{L}$ . Following a six day exposure to compounds and control conditions, organoids were fixed in 4% PFA for 15 min at room temperature. Wells were then

washed with PBS containing 100 mM glycine prior to blocking overnight in PBS containing 10% horse serum, 0.1% Bovine Serum albumin, 0.2% Triton X-100, 0.05% Tween 20 then stained with primary antibodies overnight (S1 Table) at 4°C. Secondary antibodies were then added overnight at 4°C, prior to counterstaining with Hoechst. Wells were washed with PBS then imaged on a confocal microscope, Leica TCS SP2 AOBS.

### ***In vivo* assessment of TNKS inhibitor efficacy**

All mice were obtained commercially from Charles River and then housed under UK Home Office regulations. The work described here was carried out under Home Office PPL 30/3279. *In vivo* organoid engraftment studies (also termed “organoid derived xenografts” (ODX)) were conducted using immune-deficient NOD/SCID gamma irradiated mice. For organoid transplantation, organoids were in culture for 24 h from single cells prior to subcutaneous transplantation into the right flank of the animal (one injection site per mouse). Mice were checked every 2 days for tumour growth by palpation, according to Home office regulation protocol. Palpable tumours (> 5 mm) were counted for use in Kaplan-Meier analysis. Cardiff University’s Animal Welfare and Ethical Review Body (AWERB) reviewed the plan for animal studies prior to the grant of the Home Office License (30/3279). Animals in the study described were killed by cervical dislocation (Schedule 1 method).

## **Results**

### **Establishment of tumour organoids from CRC patient material**

Surgically-resected CRC material was isolated from patients under informed consent. Cell fragments were isolated from tissue and plated within growth factor- reduced matrigel within 24 hours following surgery, adapting methods previously described by Sato et al [20]. Two different culture conditions were used as standard; “7+ basal” and “full” growth factor rich medium. Each condition was found to be optimal for a distinct subset of organoids (Fig 1A) and allowed the efficient generation of organoids from what were in some cases limited tumour cell numbers. Of 59 collected samples 48 were established in culture, a ‘take-rate’ of >81% for organoid model derivation (organoids were denoted by Isolation number, ‘Iso-’). Recent studies have similarly emphasised the requirement for different media to ensure efficient organoid generation from different patients [21].

A subset of 10 organoids was studied in more detail. Optimal culture conditions were determined on the basis of organoid formation efficiencies and visual inspection of organoid integrity. 8/10 organoid lines showed good growth in 7+ basal medium whilst 2/10 were dependent on the additional inclusion of EGF (50 ng/ml), Noggin (100 ng/ml), Nicotinamide (10 mM), A-83-01 (500 nM), SB202190 (10 μM), as well as Wnt3a- (40%) and R-spondin 1- (10%) conditioned media. The organoid medium combinations shown in Fig 1A were used for subsequent studies. Full exome sequencing showed that the subset of 10 organoids contained common genotypes found in other organoid banks (Fig 1A; S1 Appendix); [2, 34]. In particular, 80% of organoid lines harboured mutations in components of the Wnt signalling pathway, such as *APC* and  $\beta$ -*catenin* (*CTNNB1*). Iso 75 was found to harbour a mutation in *RNF43*, which is associated with an increased Frizzled (Fz) receptor expression and Wnt ligand dependence [34, 35].

CRC organoids have previously been shown to display histological features in common with the tumours from which they were derived. Paired histological samples from the organoids described were compared to their parental tumours. Distinct morphologies were observed ranging from lines that preferentially formed single epithelial cell layers with large lumens containing apoptotic cells (Fig 1B; S1 Fig) to multi-layered organoids with small



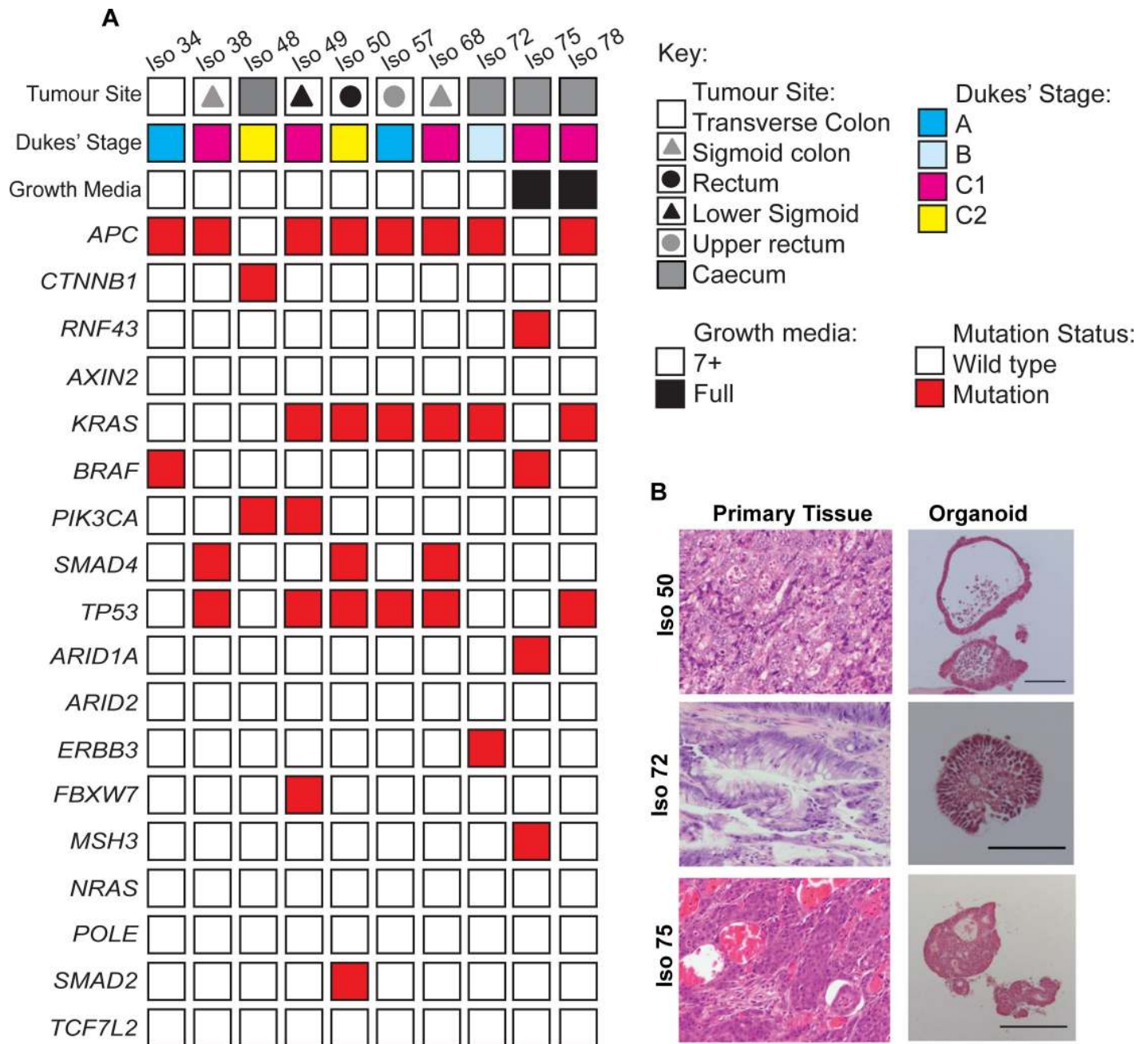


**Fig 1. Generation and establishment of tumour organoids from CRC patient material.** (A) Summary of parental tumour sites and Dukes' Stages, organoid media conditions, and mutation status of organoid lines identified in Whole Exome Sequencing analysis. (B) Representative Hematoxylin+Eosin (H&E) staining of FFPE tissue sections from primary colorectal tumour patient material and organoid counterparts. Organoids were cultured for a minimum of 6 days prior to fixation and embedding. Qualitative morphological similarities were observed between tumour and organoid pairs. Scale bar = 100 µm.

<https://doi.org/10.1371/journal.pone.0235319.g001>

indistinct lumens. The organoids frequently retained key histopathological grading features that were present within the original patient tumour epithelium. For example, Iso 72, was established from a mucinous adenocarcinoma and displayed a high percentage of mucinous vacuole structures that resembled that of the matching patient tissue. The retention of features present within primary patient tumour tissue showed that many features of tumour morphology could be retained without the need for a stromal compartment.

## Tankyrase inhibition altered the growth of patient-derived organoids

To study CRC organoid responses to a Wnt pathway inhibitor, we utilised the tankyrase inhibitor (TNKSi), C1 (Fig 2A). After six days of treatment, AXIN2 and TNKS1/2 protein levels were raised in a number of organoid lines (Fig 2B). TNKS normally targets AXIN2 and TNKS1/2 for degradation and TNKSi treatment would be expected to stabilise levels of each protein [5]. To assess the functional impact of Tankyrase inhibition on organoid growth, cell viability assays were performed for 3 organoid lines; Iso 50, Iso 72 and Iso 75. As a measure of toxicity in the normal cell setting, we also evaluated C1 response in healthy intestinal organoids. Tumour and normal intestinal organoids were digested to near-single cells, or mechanically dissociated into small fragments, embedded within growth-factor reduced Matrigel and overlaid with growth media containing the TNKSi for six days prior to measuring relative ATP levels (Cell Titer Glo 3D). C1, which has a cellular mechanistic EC<sub>50</sub> of 2nM, showed partial efficacy in reducing ATP levels and markedly different potency in the 3 CRC lines (Fig 2C–2G). C1 treatment in healthy intestinal organoids showed limited effects on metabolic activity (S3 Fig). EC<sub>50</sub> values in CRC lines ranged from 2nM to 1μM, but accurate values were hard to establish due to assay variance and also because many cells survived, even in the presence of high concentrations of compound, leading to reduced assay windows. The partial survival of organoid cells after 6 days C1 treatment suggest that long-term AXIN2 and TNKS1/2 biomarker responses might be compromised by alterations in cellular composition. Immunofluorescent staining showed reduced levels of the proliferation marker Ki67 in Iso 72 but not Iso 50 organoids suggesting that reduced proliferation contributed to the lower ATP levels observed (Fig 2H and 2I).

## Multi-parametric phenotypic profiling of organoids in 3D to classify responses to Tankyrase inhibition

To better understand the TNKSi partial efficacy, a novel multi-parametric 3D image workflow analysis was used to characterise the morphological effects of the responses. Three Tankyrase 1/2 (TNKS1/2) small molecule inhibitors were used that differed over 3 orders of magnitude in their potency (C1; 2nM, C2; 36nM, C3; 319nM Fig 2A). Organoids were seeded and treated as previously for 6 days prior to fixation and staining with rhodamine-phalloidin (F-actin) and Hoechst 33258 (DNA). Images were acquired using a high-content wide-field fluorescence microscope as described previously [32, 36].

To characterise phenotypes, OMiner™ software (OcellO™) was used to extract morphological features from 2D projections of the F-actin and nuclei-derived image stacks to generate masks of individual organoids, internal lumen structures and nuclei. Image segmentation was used to distinguish components of both channels and minimise any background signal (Fig 3A; S4 Fig). Overall shape and fluorescence intensity of individual organoid structures were extracted on a well-by-well basis to generate approximately 600 quantified features. Such features included information in regards to shape, size, boundaries and branching of organoid lumens and nuclear shape.

To identify optimum features that could classify TNKSi responses, feature training and Euclidian distance calculations were performed on each data set as previously described [36]. This reduced features into key differentiating components to generate a measure of distance between highest C1 TNKSi doses and negative control (DMSO, 0.1%) conditions. The feature collection that describes the compound-induced morphological change differs per organoid model, but most frequently included organoid size changes, lumen shape and size, appearance of dead cells and changes in nucleus morphology related to growth reduction, cell organization and cell death induction (S5 Fig).

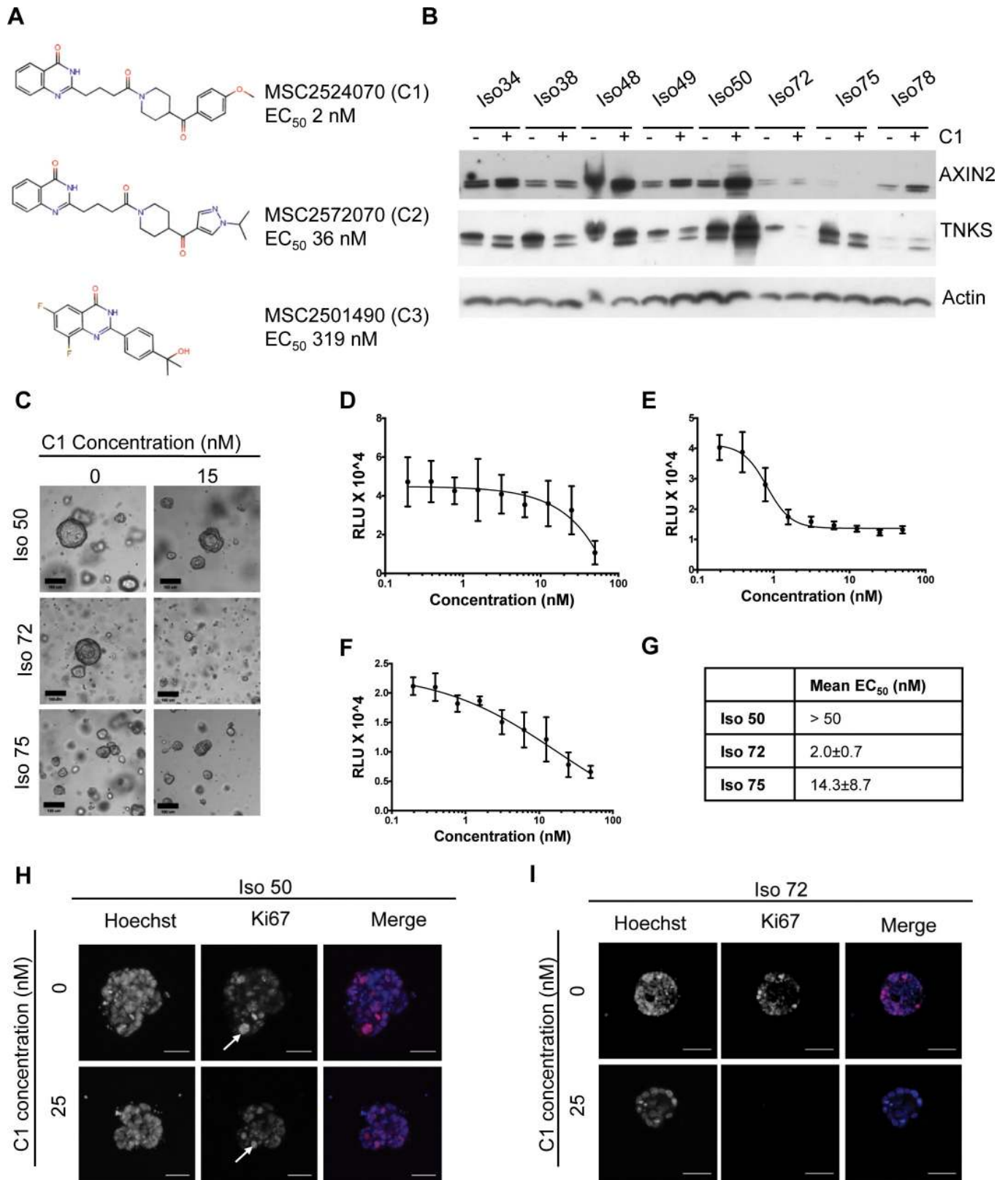


**Fig 2. Assessing the effects of Tankyrase inhibition on overall organoid viability.** (A) Structures of three tankyrase inhibitors: MSC2524070A (C1), MSC2572070A (C2) and MSC2501490A (C3), with corresponding EC<sub>50</sub> values. (B) Western blot of eight organoid lines treated with C1 (15 nM) and harvested

after 6 days. (C) Representative images of organoids treated with C1 (15 nM) or DMSO (scale bar = 100  $\mu$ m). (D, E, F) Dose-response curves of organoids treated with C1 for six days. Organoids previously established in suitable culture conditions were enzymatically digested to single cells and overlaid with media containing a dose range of drug (0.195 nM– 50 nM), or a DMSO control (0.1% in media). Cell Titer Glo 3D readouts were performed in triplicates for Iso 50 (D), Iso 72 (E), Iso 75 (F). (G)  $EC_{50}$  values, obtained from ( $n = 3$ ) experiments. Data are presented as mean  $\pm$  S.E.M. (H, I) Representative immunofluorescent staining of a proliferation marker in organoids. Iso 50 (H) and Iso 72 (I) with differential sensitivity to TNKSi were treated with C1 (25 nM) or DMSO (0.1%) control for 6 days, fixed and stained with Ki67. Arrows indicate proliferating cell within the organoid, Ki67 positive-cells in Iso 72 only when treated with C1 (scale bar = 50  $\mu$ m).

<https://doi.org/10.1371/journal.pone.0235319.g002>

The morphometric analysis showed that TNKS inhibition resulted in phenotypic alterations in Iso 38, Iso 72, Iso 75 and Iso 78 (Fig 3B). Importantly, the cellular morphometric responses correlated with known cellular  $EC_{50}$  values across a range of potencies. Compounds C1, C2 and C3 that had  $EC_{50}$  values of 2 nM, 36 nM and 319 nM (Table 1) also showed the expected separation of  $EC_{50}$  activities in the organoid morphometric assays, suggesting that observed

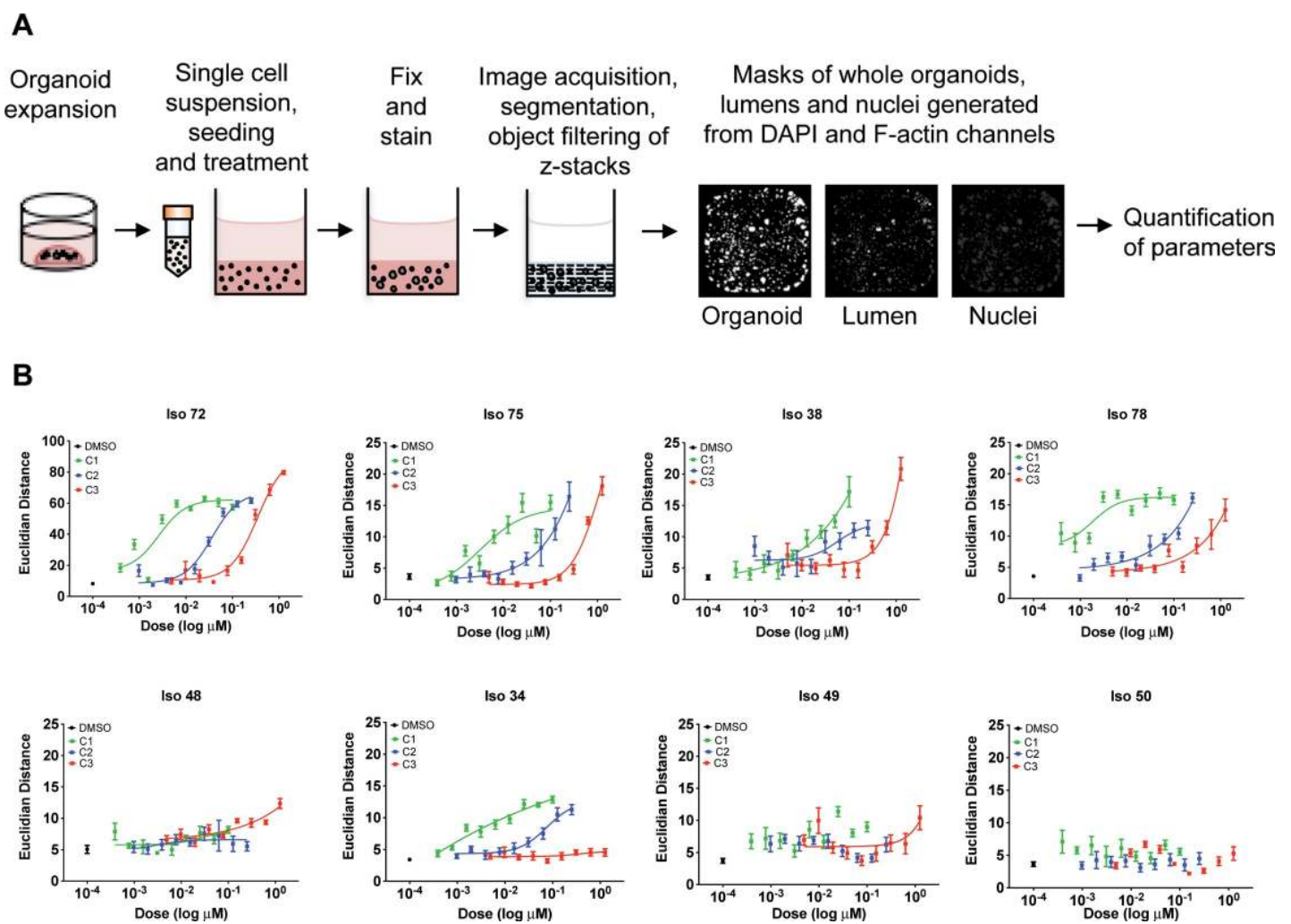


**Fig 3. 3D image analysis demonstrates target affinity of tankyrase inhibitors in organoids.** (A) Flow diagram of high-content multi-parametric image screen process. (B) Dose response curves acquired from high content imaging screen. Organoids were seeded as single cells in 384 well plates and exposed to Tankyrase inhibitors C1, C2, C3 for six days. Individual morphological measurements were generated from DAPI and F-actin channels. Principal component analysis was used to select the top 10 most discriminating features to separate compound-induced phenotypes between high and low doses of Tankyrase inhibitors. Selected parameters were used for feature space training, whereby Euclidean distance metrics were calculated between high and low doses of each compound for each organoid line. Euclidean distances were used as an indicator of similarity between low and high doses, with a low distance indicative of high phenotypic similarity between conditions. Data are presented as mean Euclidean distance from 8 replicate wells  $\pm$  S.D.

<https://doi.org/10.1371/journal.pone.0235319.g003>

**Table 1. Summary of EC<sub>50</sub> values obtained by morphometric analysis.**

EC <sub>50</sub> (nM)	C1	C2	C3
Cell line	2	36	300
Iso 34	3	75	No Fit
Iso 38	9	55	2000
Iso 48	No fit	No fit	No fit
Iso 49	No fit	No fit	No fit
Iso 50	No fit	No fit	No fit
Iso 72	2.6	36	346
Iso 75	3	31	1060
Iso 78	1.8	30	400

<https://doi.org/10.1371/journal.pone.0235319.t001>

effects were as a result of targeted inhibition of TNKS. Iso 72, Iso 75 and Iso 78, showed clear differential dose-dependent potency for three compounds. Two additional lines, Iso 38 and Iso 34 showed partial separation of their morphological responses in line with the order of cellular potency. Iso 50, Iso 48 and Iso49 showed no discernible responses. The effect sizes of the morphometric responses compared very favourably with the noisier data from the ATP assays (Fig 2C).

Iso 75 and Iso 78 organoids required ‘full’ medium containing exogenous Wnt and R-spondin ligands for expansion in culture. Whole exome sequencing revealed that Iso 75 harboured an *RNF43* mutation (Fig 1A), which would likely yield organoids that require Wnt signalling at the receptor level—upstream of the Axin-containing  $\beta$ -catenin turnover complex [35]. However, both Iso 72 and Iso 38 grew independently of Wnt and R-spondin suggesting that TNKSi sensitivity is not necessarily as a result of exogenous Wnt conditions. Collectively, this data indicates that 3D image based assays provide an accurate identification and quantification of organoid responses to Wnt signalling modulators.

### Sensitivity to Tankyrase inhibitors was associated with drug-induced suppression of stem cell markers

Tankyrases promote the degradation of Axin, inducing  $\beta$ -catenin stabilization and activation of Wnt signalling [5]. We therefore investigated the impact of TNKS inhibition on components of the Wnt signalling pathway in the organoid lines. The cellular distribution of  $\beta$ -catenin was assessed by immunofluorescence in organoids treated with C1 (15 nM for 6 days). TNKS inhibition reduced total  $\beta$ -catenin levels in both TNKS sensitive (Iso 72 and Iso 75) and non-sensitive lines (Iso 50; Fig 4A) suggesting that TNKSi were biochemically active in all organoid lines. Quantitative RT-PCR was used to analyse gene expression changes in response to TNKSi treatment for 6 days. Expression of *DKK1* and *ASCL2*, two direct  $\beta$ -catenin target genes [37], were reduced in all three lines although the effect size was greater in *ASCL2* levels of the TNKSi-sensitive lines Iso 72 and Iso 75 than in the TNKSi-insensitive line Iso 50 ( $p < 0.001$ , Fig 4B). Taken together, this suggested that the loss of  $\beta$ -catenin was linked to changes in gene expression, but not necessarily to functional responses. Changes in gene expression which did correlate with functional TNKSi sensitivity included reductions in the expression of the intestinal stem cell marker *LGR5* and the upregulation of cytokeratin 20 (*KRT20*) (Fig 4B; S6 Fig), suggesting that tankyrase inhibition may induce differentiation as has previously been shown with CRC cell lines [8].

*Lgr5* immunostaining in the Iso 50, Iso 72 and Iso 75 lines correlated with the qRT-PCR results (S6 Fig). *Lgr5*-positive cells were detected in both TNKSi-treated and untreated Iso 50

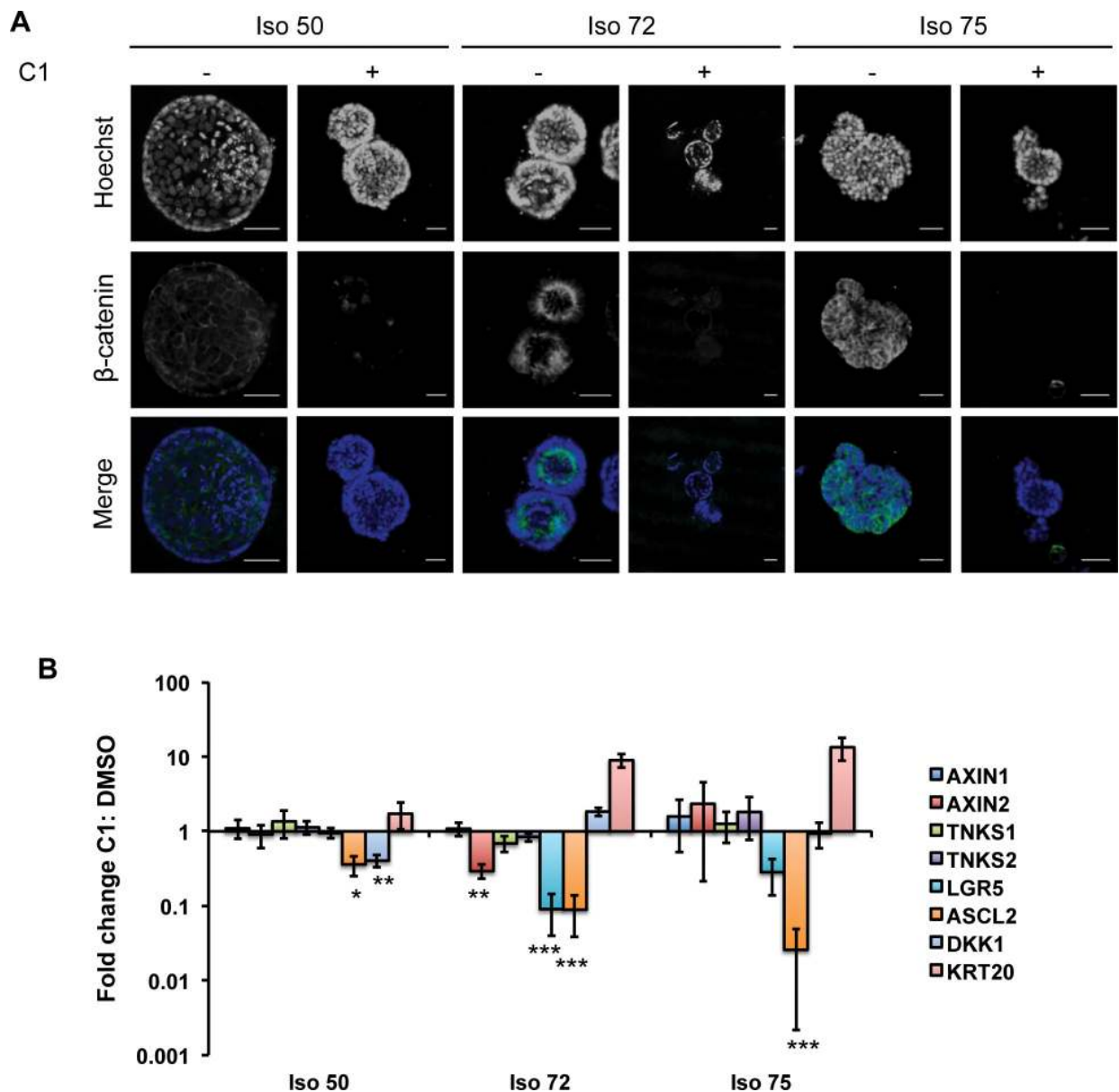


**Fig 4. Tankyrase inhibition alters the proportion of stemness in CRC organoids.** (A) Representative confocal images of organoids stained with a  $\beta$ -catenin antibody following six days of exposure to C2 or control (DMSO, 0.1%) showing a reduction in the intensity and numbers of cells showing  $\beta$ -catenin positivity following treatment (scale bar = 50  $\mu$ m). (B) Quantitative real-time PCR analysis of relative mRNA expression of intestinal epithelial markers from organoids (Iso 50, Iso 72, Iso 75) cultured with tankyrase inhibitor C1 (15 nM, 6 days) or DMSO (0.1%). Markers associated with intestinal stem cell activity (LGR5, ASCL2), differentiation (KRT20, DKK1) alongside other members of the Wnt-signalling pathway were determined, with mRNA expression normalized to control conditions. Experiments were performed in biological repeats ( $n = 3$ ) with error bars indicative of S.E.M (\*\*\*,  $p \leq 0.001$ ; \*\*,  $p \leq 0.01$ ; \*,  $p \leq 0.05$ , Paired Student's t-test with Bonferroni correction).

<https://doi.org/10.1371/journal.pone.0235319.g004>

organoids, while Iso 72 and Iso 75 to TNKSi showed reductions in expression following TNKSi treatment. Taken together, these results suggest that the pharmacological inhibition of TNKS results in an overall reduction of Wnt/ $\beta$ -catenin signalling in both TNKSi-sensitive and resistant organoid lines and that phenotypic responses could not be simply predicted based on the expression of biomarkers. The best overall biomarker of organoid response may instead be functional morphometric readouts, perhaps as a consequence of differential cellular responses to the compounds being studied.

## Assessing the effects of Tankyrase inhibition in a patient organoid-derived xenograft (ODX) model

The presence of cancer stem cells is often identified by transplantation of tumour cells within immune-deficient animal models and subsequent formation of tumours [38]. To assess whether both functional and phenotypic effects of TNKSi within the sensitive organoids would translate to a reduction in tumour growth *in vivo*, an organoid-derived xenograft model was generated from the TNKSi-sensitive line, Iso 75. Organoids were digested to single cells, plated in Matrigel and immediately treated with TNKS inhibitor C1 (30 nM) or vehicle control (DMSO, 0.1%) for 24 hours. Based on previous work showing rapid responses to Wnt pathway inhibition [39], it was hypothesised that the pre-treatment of organoids would result in a transcriptional effect as a result of Wnt signalling inhibition, altering the cancer stem cell function of cells within the organoids.

Following treatment, small organoids were injected orthotopically into the flanks of 16 gamma-irradiated Non-Obese Diabetic/Severe Combined Immunodeficiency (NOD/SCID/ $\gamma$ ) mice, at one injection site per mouse (Fig 5A). Tumours grew from the injected organoids at 100% of sites injected. However, TNKSi pre-treated organoids showed significantly delayed tumour formation by comparison with vehicle control (Fig 5B; Log Mantel-Cox test

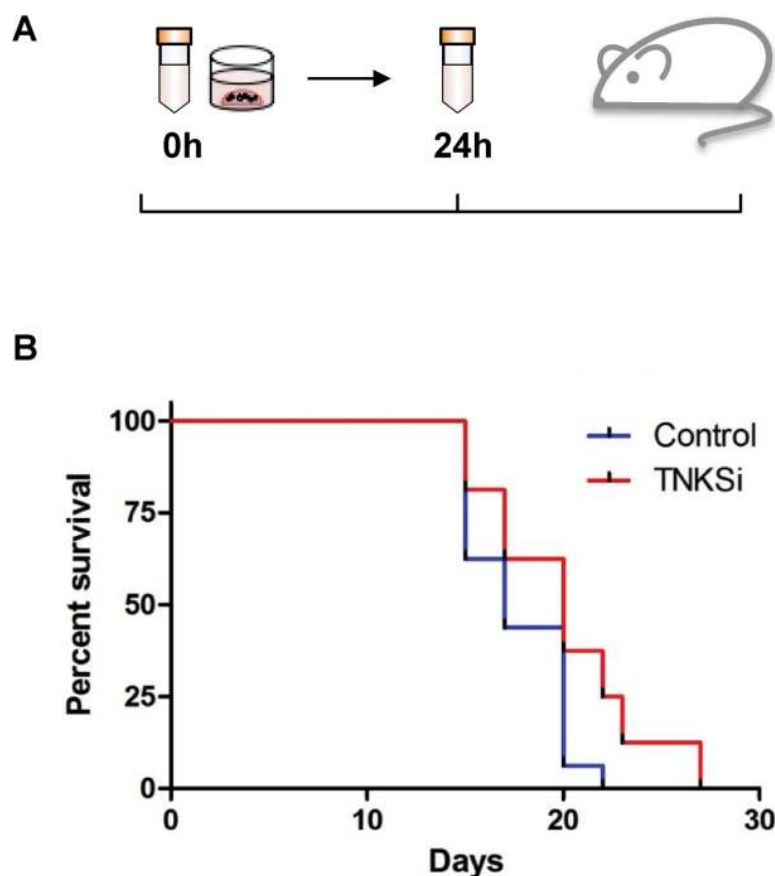


**Fig 5. TNKSi-treated organoids enhance survival in an organoid-derived xenograft (ODX) mouse model.** (A) Schematic diagram depicting organoid transplantation into mice. (B) A cohort of 16 NOD/SCID/ $\gamma$ -irradiated mice were injected with pre-treated (30 nM C2 for 24 hours) Iso 75 organoids, or control (0.1% DMSO, 24 hours) organoids within one injection site per mouse. TNKSi-treated organoids showed a significant delayed formation of tumours compared to control conditions (Log-Rank (Mantel-Cox) test  $P = 0.032$ ).

<https://doi.org/10.1371/journal.pone.0235319.g005>

$p = 0.032$ ), suggesting that the 24 hour TNKSi exposure was sufficient to reduce the capacity of transplanted organoids to form tumours.

## Discussion

3D organoids represent an attractive platform for the capture of the effects of therapies targeting signalling pathways involved in the regulation of complex morphometric interactions that are not well represented in clonal 2D culture. Here, compounds targeting the Wnt/ $\beta$ -catenin pathway were studied in patient derived CRC organoids using image-based analyses as previously described [32, 36]. Numerous morphometric features, such as the distance of the matrix to central lumens and the number of nuclei per structure were quantified using automated algorithms. Due to their biological complexity, multi-parameter sets of organoid-responses may be able to characterise treatment-induced phenotypes that are linked to underlying signalling and cell biological processes. For example, changes in the activity of regulators of cell lineage will likely be reflected in alterations to the spatial organisation of cell types and organoid morphology organoids [40]. However, predictions as to how any particular morphological response is driven by alterations to specific biological mechanisms will require the development of predictive multiscale mathematical models of organoid morphology and signalling pathways [41].

Overall, morphometric analyses were found to improve assay windows by comparison with biochemical assays, most likely by aggregating multiple phenotypic responses that sensitively discriminate responses to drug treatments [32, 42].

The identification of a set of morphometric parameters that accurately distinguish between compounds of different potency allowed putative biomarkers of TNKSi sensitivity to be compared with organoid phenotypic responses. Single parameter functional readouts such as TNKSi-induced alterations in ATP levels showed a reduced effect size by comparison with the morphometric responses. Alterations in a range of alternative biomarkers correlated poorly with morphometric responses. Alterations in the expression of stem cell marker genes including *ASCL2* and *LGR5* correlated with cellular responses, but larger-scale studies will be required to determine whether panels of gene expression markers reliably predict organoid (and ultimately patient) responses. Confounding factors in these analyses are likely to be the levels of stem cell gene expression, variation in the 'stemness' of tumours and the proportion of cancer stem cells within tumour and corresponding organoid populations. Each of these properties themselves are likely to be dynamically altered following compound treatment, requiring detailed time-course analyses to deconvolute. By contrast, changes to developmental trajectories induced by compounds such as TNKSi will leave a permanent record in each organoid's morphological structure.

Morphometric assays showed that Iso75, a line that required Wnt3a and R-spondin for growth (mutant for *RNF43* mutant and APC wild type), was sensitive to TNKSi as expected [35]. However, a simple correlation between Wnt-dependence in culture and TNKSi sensitivity was not observed since 5 out of the 8 lines examined showed morphometric responses that tracked the cellular potency of the TNKS inhibitors (Fig 3B). In particular, clear phenotypic responses were observed in Iso 72 and 78, both of which were APC mutant and only one of which required Wnt/Rspo-conditioned medium for growth.

Whilst it is mechanistically challenging to directly link Wnt inhibition via morphometric responses to alterations in stem cell cycling, pre-treatment of a TNKSi sensitive organoid line for 24h *in vitro* delayed subsequent tumour formation *in vivo* following transplantation. Taken together with the reductions in Wnt target gene expression and  $\beta$ -catenin levels, this would



suggest that modulation of Wnt signalling in a sensitive line was sufficient to limit the stem-like signature of organoid cell populations.

Despite the benefits of using the morphometric assay formats described here to identify clear responses to Wnt modulating therapies, key challenges remain to be addressed. From a clinical perspective, further detailed investigation of Wnt modulators will be required to determine whether TNKS inhibitors can provide clinical benefit. Toxicity remains an issue with inhibitors [8], however recent studies have suggested these might be reversible [43], such that careful timing of Wnt-inhibitor treatment in combination with standard-of-care therapies could identify rational therapeutic opportunities. When strategies targeting cancer stem cells have been further developed, a robust *in vitro* readout such as organoid morphology may be able to identify those patients who would benefit the most. Lastly, the imaging pipeline described might be usefully applied in drug discovery screens, enabling the detection of compounds that might otherwise have been rejected for lack of efficacy during pre-clinical drug testing.

## Supporting information

### S1 Checklist.

(DOCX)

**S1 Fig. Hematoxylin & Eosin staining.** Hematoxylin & Eosin (H & E) staining of FFPE tissue sections derived from primary colorectal tumour patient material, with organoid counterparts. Scale bar = 100  $\mu\text{m}$ .

(DOCX)

**S2 Fig. Immunoblot scans.** Full scans of immunoblots. Related to Fig 2B. Organoids and cell line controls were treated with TNKSi C1 (organoids 15 nM, cell line 50nM) and blotted for TNKS1/2 top or Axin2 bottom. Novex Sharp pre-stained protein standards (Invitrogen; LC5800) were loaded as per manufacturers instructions.

(DOCX)

**S3 Fig. Healthy intestinal organoids treated with C1.** (A) Representative images of healthy intestinal organoids treated with C1 (12.5 nM, 100 nM) or DMSO (scale bar = 100  $\mu\text{m}$ ). (B) Dose-response curves of organoids treated with C1 for six days. Organoids previously established in suitable culture conditions were passaged by mechanical trituration into small (<100  $\mu\text{m}$ ) structures, overlaid with media to allow recovery for 24 hours, then treated with a dose range of C1 (0.31 nM– 100 nM) or DMSO control (0.1% in media). Organoids were treated for a total of 6 days with metabolic activity determined using Cell Titer Glo 3D, with readings normalized to DMSO control (100%), n = 3 independent experiments, with results shown as mean  $\pm$  S.D.

(DOCX)

**S4 Fig. Image analysis projections.** Representative images of organoids exposed to low and high dose TNKSi (C1, C2 and C3 for 6 days) after image analysis. Projections of the Hoechst (Blue) and Phalloidin-rhodamine (Red) signal are overlaid with the cell and lumen mask (Green). The images show 10% of the original image. Scale bar = 500  $\mu\text{m}$ .

(DOCX)

**S5 Fig. Z-projection images.** Representative images of organoids (Iso 50, Iso 72 and Iso 75) exposed to high dose TNKSi (C1; 100 nM, C2; 250 nM and C3; 1.25 $\mu\text{M}$ , 6 days) versus DMSO control after image analysis. Z-Projections of the Hoechst (Blue) and Phalloidin-rhodamine (Red) signal are overlaid with the organoid and lumen mask (yellow and green). Individual z-

section masks illustrate changes in morphology of organoids in treatment versus DMSO conditions. The images show 10% of the original image. Scale bar = 500  $\mu\text{m}$ .

(DOCX)

**S6 Fig. Organoid confocal images.** A Representative confocal images of organoids stained with an Lgr5 and Cytokeratin 20 antibody following six days of exposure to C1 (15 nM) or control (DMSO, 0.1%). Sensitive organoids demonstrated an overall reduction in the number of Lgr5 positive cells and increase in Cytokeratin 20 positive cells following treatment.

(DOCX)

**S1 Table. Primary antibodies used for fluorescence microscopy.**

(DOCX)

**S2 Table. Primers used for qRT-PCR by SYBR green.**

(DOCX)

**S1 Appendix. Whole exome sequencing analysis for each organoid line.** The mutations reported in the table are those found to have been previously described as likely oncogenic and curated within the COSMIC and cBioportal databases.

(DOCX)

## Acknowledgments

We acknowledge all members of the University Hospital of Wales (UHW) Colorectal surgical team and UHW Histopathology team. The authors would like to thank the Wales Cancer Bank for providing access to all patient material and to patients for providing their consent to this study. We also acknowledge members of the Bioimaging facility at Cardiff School of Biosciences for technical support. We acknowledge our colleagues at the Wales Gene Park for their insight and expertise that assisted this research, and their technical and bioinformatic support in generating the NGS data. Wales Gene Park is a Health and Care Research Wales funded infrastructure support group. We acknowledge the guidance and expertise of Laura Thomas, Hannah West and Elena Meuser of the Inherited Tumour Syndrome Research Group within the School of Medicine, Cardiff University with bioinformatic workflows and CRC genetics. We acknowledge the support of Cellesce Ltd. We thank Victoria Marsh Durban and Anika Offergeld for manuscript proof reading and corrections. A.R.C passed away before the submission of the final version of this manuscript but was aware of the results. T.C.D accepts responsibility for the integrity and validity of the data collected and analysed.

## Author Contributions

**Conceptualization:** Luned M. Badder, Andrew J. Hollins, Alan R. Clarke, Dirk Wienke, Leo S. Price, Paul H. Shaw, Trevor C. Dale.

**Data curation:** Luned M. Badder, Bram Herpers, Kuan Yan, Marc Naven, Kevin E. Ashelford.

**Formal analysis:** Luned M. Badder, Andrew J. Hollins, Bram Herpers, Kuan Yan, Kenneth B. Ewan, Mairian Thomas, Jennifer R. Shone, Marc Naven, Kevin E. Ashelford.

**Funding acquisition:** Alan R. Clarke, Paul H. Shaw, Trevor C. Dale.

**Investigation:** Luned M. Badder, Andrew J. Hollins, Bram Herpers, Kuan Yan, Kenneth B. Ewan, Mairian Thomas, Jennifer R. Shone, Delyth A. Badder, Christina Esdar, Hans-Peter Buchstaller.

**Methodology:** Luned M. Badder, Andrew J. Hollins, Kenneth B. Ewan, Sylvia Boj, Bahar Ramezanpour.

**Project administration:** Luned M. Badder, Leo S. Price, Paul H. Shaw, Trevor C. Dale.

**Resources:** Bram Herpers, Kuan Yan, Kenneth B. Ewan, Delyth A. Badder, Marc Naven, Kevin E. Ashelford, Rachel Hargest, Christina Esdar, Hans-Peter Buchstaller, J. Mark Treherne, Sylvia Boj, Bahar Ramezanpour, Dirk Wienke.

**Software:** Bram Herpers, Kuan Yan, Marc Naven, Kevin E. Ashelford.

**Supervision:** Alan R. Clarke, Paul H. Shaw, Trevor C. Dale.

**Validation:** Luned M. Badder, Andrew J. Hollins, Kenneth B. Ewan, Jennifer R. Shone, Alan R. Clarke.

**Visualization:** Luned M. Badder, Andrew J. Hollins.

**Writing – original draft:** Luned M. Badder.

**Writing – review & editing:** Andrew J. Hollins, Bram Herpers, Mairian Thomas, Dirk Wienke, Leo S. Price, Trevor C. Dale.

## References

1. Giles RH, van Es JH, Clevers H. Caught up in a Wnt storm: Wnt signaling in cancer. *Biochim Biophys Acta*. 2003; 1653: 1–24. [https://doi.org/10.1016/s0304-419x\(03\)00005-2](https://doi.org/10.1016/s0304-419x(03)00005-2) PMID: 12781368
2. The Cancer Genome Atlas N, Muzny DM, Bainbridge MN, Chang K, Dinh HH, Drummond JA, et al. Comprehensive molecular characterization of human colon and rectal cancer. *Nature*. 2012; 487: 330. <https://doi.org/10.1038/nature11252> PMID: 22810696
3. Amit S, Hatzubai A, Birman Y, Andersen JS, Ben-Shushan E, Mann M, et al. Axin-mediated CKI phosphorylation of beta-catenin at Ser 45: a molecular switch for the Wnt pathway. *Genes Dev*. 2002; 16: 1066–76. <https://doi.org/10.1101/gad.230302> PMID: 12000790
4. Van der Flier LG, Sabates-Bellver J, Oving I, Haegebarth A, De Palo M, Anti M, et al. The Intestinal Wnt/TCF Signature. *Gastroenterology*. 2007; 132: 628–32. <https://doi.org/10.1053/j.gastro.2006.08.039> PMID: 17320548
5. Huang S-MA, Mishina YM, Liu S, Cheung A, Stegmeier F, Michaud GA, et al. Tankyrase inhibition stabilizes axin and antagonizes Wnt signalling. *Nature*. 2009; 461: 614. <https://doi.org/10.1038/nature08356> PMID: 19759537
6. Zhang LS, Lum L. Chemical Modulation of WNT Signaling in Cancer. *Prog Mol Biol Transl Sci*. 2018; 153: 245–69. <https://doi.org/10.1016/bs.pmbts.2017.11.008> PMID: 29389519
7. Clarke PA, Ortiz-Ruiz MJ, TePoele R, Adeniji-Popoola O, Box G, Court W, et al. Assessing the mechanism and therapeutic potential of modulators of the human Mediator complex-associated protein kinases. *Elife*. 2016; 5. <https://doi.org/10.7554/eLife.20722> PMID: 27935476
8. Lau T, Chan E, Callow M, Waaler J, Boggs J, Blake RA, et al. A novel tankyrase small-molecule inhibitor suppresses APC mutation-driven colorectal tumor growth. *Cancer Res*. 2013; 73: 3132–44. <https://doi.org/10.1158/0008-5472.CAN-12-4562> PMID: 23539443
9. Wu X, Luo F, Li J, Zhong X, Liu K. Tankyrase 1 inhibitor XAV939 increases chemosensitivity in colon cancer cell lines via inhibition of the Wnt signaling pathway. *Int J Oncol*. 2016; 48: 1333–40. <https://doi.org/10.3892/ijo.2016.3360> PMID: 26820603
10. Waaler J, Machon O, Tumova L, Dinh H, Korinek V, Wilson SR, et al. A novel tankyrase inhibitor decreases canonical Wnt signaling in colon carcinoma cells and reduces tumor growth in conditional APC mutant mice. *Cancer Res*. 2012; 72: 2822–32. <https://doi.org/10.1158/0008-5472.CAN-11-3336> PMID: 22440753
11. Mizutani A, Yashiroda Y, Muramatsu Y, Yoshida H, Chikada T, Tsumura T, et al. RK-287107, a potent and specific tankyrase inhibitor, blocks colorectal cancer cell growth in a preclinical model. *Cancer Sci*. 2018; 109: 4003–14. <https://doi.org/10.1111/cas.13805> PMID: 30238564
12. Gunaydin H, Gu Y, Huang X. Novel Binding Mode of a Potent and Selective Tankyrase Inhibitor. *PLOS ONE*. 2012; 7: e33740. <https://doi.org/10.1371/journal.pone.0033740> PMID: 22438990

13. Waaler J, Machon O, von Kries JP, Wilson SR, Lundenes E, Wedlich D, et al. Novel synthetic antagonists of canonical Wnt signaling inhibit colorectal cancer cell growth. *Cancer Res.* 2011; 71: 197–205. <https://doi.org/10.1158/0008-5472.CAN-10-1282> PMID: [21199802](https://pubmed.ncbi.nlm.nih.gov/21199802/)
14. James RG, Davidson KC, Bosch KA, Biechele TL, Robin NC, Taylor RJ, et al. WIKI4, a Novel Inhibitor of Tankyrase and Wnt/ $\beta$ -Catenin Signaling. *PLOS ONE.* 2012; 7: e50457. <https://doi.org/10.1371/journal.pone.0050457> PMID: [23227175](https://pubmed.ncbi.nlm.nih.gov/23227175/)
15. Okada-Iwasaki R, Takahashi Y, Watanabe Y, Ishida H, Saito J, Nakai R, et al. The Discovery and Characterization of K-756, a Novel Wnt/ $\beta$ -Catenin Pathway Inhibitor Targeting Tankyrase. *Mol Cancer Ther.* 2016; 15: 1525–34. <https://doi.org/10.1158/1535-7163.MCT-15-0938> PMID: [27196752](https://pubmed.ncbi.nlm.nih.gov/27196752/)
16. Shultz MD, Cheung AK, Kirby CA, Firestone B, Fan J, Chen CH, et al. Identification of NVP-TNKS656: the use of structure–efficiency relationships to generate a highly potent, selective, and orally active tankyrase inhibitor. *J Med Chem.* 2013; 56: 6495–511. <https://doi.org/10.1021/jm400807n> PMID: [23844574](https://pubmed.ncbi.nlm.nih.gov/23844574/)
17. Thorvaldsen TE. Targeting Tankyrase to Fight WNT-dependent Tumours. *Basic Clin Pharmacol Toxicol.* 2017; 121: 81–8. <https://doi.org/10.1111/bcpt.12786> PMID: [28371398](https://pubmed.ncbi.nlm.nih.gov/28371398/)
18. Novellademunt L, Antas P, Li VS. Targeting Wnt signaling in colorectal cancer. A Review in the Theme: Cell Signaling: Proteins, Pathways and Mechanisms. *Am J Physiol Cell Physiol.* 2015; 309: C511–21. <https://doi.org/10.1152/ajpcell.00117.2015> PMID: [26289750](https://pubmed.ncbi.nlm.nih.gov/26289750/)
19. Gillet JP, Varma S, Gottesman MM. The clinical relevance of cancer cell lines. *J Natl Cancer Inst.* 2013; 105: 452–8. <https://doi.org/10.1093/jnci/djt007> PMID: [23434901](https://pubmed.ncbi.nlm.nih.gov/23434901/)
20. Sato T, Stange DE, Ferrante M, Vries RG, Van Es JH, Van den Brink S, et al. Long-term expansion of epithelial organoids from human colon, adenoma, adenocarcinoma, and Barrett's epithelium. *Gastroenterology.* 2011; 141: 1762–72. <https://doi.org/10.1053/j.gastro.2011.07.050> PMID: [21889923](https://pubmed.ncbi.nlm.nih.gov/21889923/)
21. Fujii M, Shimokawa M, Date S, Takano A, Matano M, Nanki K, et al. A Colorectal Tumor Organoid Library Demonstrates Progressive Loss of Niche Factor Requirements during Tumorigenesis. *Cell Stem Cell.* 2016; 18: 827–38. <https://doi.org/10.1016/j.stem.2016.04.003> PMID: [27212702](https://pubmed.ncbi.nlm.nih.gov/27212702/)
22. Weeber F, van de Wetering M, Hoogstraat M, Dijkstra KK, Krijgsman O, Kuilman T, et al. Preserved genetic diversity in organoids cultured from biopsies of human colorectal cancer metastases. *Proc Natl Acad Sci U S A.* 2015; 112: 13308–11. <https://doi.org/10.1073/pnas.1516689112> PMID: [26460009](https://pubmed.ncbi.nlm.nih.gov/26460009/)
23. Pauli C, Hopkins BD, Prandi D, Shaw R, Fedrizzi T, Sboner A, et al. Personalized In Vitro and In Vivo Cancer Models to Guide Precision Medicine. *Cancer Discov.* 2017; 7: 462–77. <https://doi.org/10.1158/2159-8290.CD-16-1154> PMID: [28331002](https://pubmed.ncbi.nlm.nih.gov/28331002/)
24. Menon M, Elliott R, Bowers L, Balan N, Rafiq R, Costa-Cabral S, et al. A novel tankyrase inhibitor, MSC2504877, enhances the effects of clinical CDK4/6 inhibitors. *Sci Rep.* 2019; 9: 201. <https://doi.org/10.1038/s41598-018-36447-4> PMID: [30655555](https://pubmed.ncbi.nlm.nih.gov/30655555/)
25. Parry-Jones A, Spary L.K. The Wales Cancer Bank (WCB). *Open Journal of Bioresources.* 2018; 5: 10. <https://doi.org/10.5334/ojb.46>
26. Ootani A, Li X, Sangiorgi E, Ho QT, Ueno H, Toda S, et al. Sustained in vitro intestinal epithelial culture within a Wnt-dependent stem cell niche. *Nat Med.* 2009; 15: 701–6. <https://doi.org/10.1038/nm.1951> PMID: [19398967](https://pubmed.ncbi.nlm.nih.gov/19398967/)
27. Li H, Durbin R. Fast and accurate short read alignment with Burrows-Wheeler transform. *Bioinformatics.* 2009; 25: 1754–60. <https://doi.org/10.1093/bioinformatics/btp324> PMID: [19451168](https://pubmed.ncbi.nlm.nih.gov/19451168/)
28. Li H, Handsaker B, Wysoker A, Fennell T, Ruan J, Homer N, et al. The Sequence Alignment/Map format and SAMtools. *Bioinformatics.* 2009; 25: 2078–9. <https://doi.org/10.1093/bioinformatics/btp352> PMID: [19505943](https://pubmed.ncbi.nlm.nih.gov/19505943/)
29. McKenna A, Hanna M, Banks E, Sivachenko A, Cibulskis K, Kernysky A, et al. The Genome Analysis Toolkit: a MapReduce framework for analyzing next-generation DNA sequencing data. *Genome Res.* 2010; 20: 1297–303. <https://doi.org/10.1101/gr.107524.110> PMID: [20644199](https://pubmed.ncbi.nlm.nih.gov/20644199/)
30. DePristo MA, Banks E, Poplin R, Garimella KV, Maguire JR, Hartl C, et al. A framework for variation discovery and genotyping using next-generation DNA sequencing data. *Nature Genetics.* 2011; 43: 491. <https://doi.org/10.1038/ng.806> PMID: [21478889](https://pubmed.ncbi.nlm.nih.gov/21478889/)
31. McLaren W, Gil L, Hunt SE, Riat HS, Ritchie GR, Thormann A, et al. The Ensembl Variant Effect Predictor. *Genome Biol.* 2016; 17: 122. <https://doi.org/10.1186/s13059-016-0974-4> PMID: [27268795](https://pubmed.ncbi.nlm.nih.gov/27268795/)
32. Di Z, Klop MJD, Rogkoti V-M, Le Dévédec SE, van de Water B, Verbeek FJ, et al. Ultra High Content Image Analysis and Phenotype Profiling of 3D Cultured Micro-Tissues. *PLOS ONE.* 2014; 9: e109688. <https://doi.org/10.1371/journal.pone.0109688> PMID: [25289886](https://pubmed.ncbi.nlm.nih.gov/25289886/)
33. Booi TH, Bange H, Leonhard WN, Yan K, Fokkelman M, Kunnen SJ, et al. High-Throughput Phenotypic Screening of Kinase Inhibitors to Identify Drug Targets for Polycystic Kidney Disease. *SLAS Discov.* 2017; 22: 974–84. <https://doi.org/10.1177/2472555217716056> PMID: [28644734](https://pubmed.ncbi.nlm.nih.gov/28644734/)

34. van de Wetering M, Francies HE, Francis JM, Bounova G, Iorio F, Pronk A, et al. Prospective derivation of a living organoid biobank of colorectal cancer patients. *Cell*. 2015; 161: 933–45. <https://doi.org/10.1016/j.cell.2015.03.053> PMID: 25957691
35. Koo B-K, Spit M, Jordens I, Low TY, Stange DE, van de Wetering M, et al. Tumour suppressor RNF43 is a stem-cell E3 ligase that induces endocytosis of Wnt receptors. *Nature*. 2012; 488: 665. <https://doi.org/10.1038/nature11308> PMID: 22895187
36. Sandercock AM, Rust S, Guillard S, Sachsenmeier KF, Holoweckyj N, Hay C, et al. Identification of anti-tumour biologics using primary tumour models, 3-D phenotypic screening and image-based multi-parametric profiling. *Mol Cancer*. 2015; 14: 147. <https://doi.org/10.1186/s12943-015-0415-0> PMID: 26227951
37. Niida A, Hiroko T, Kasai M, Furukawa Y, Nakamura Y, Suzuki Y, et al. DKK1, a negative regulator of Wnt signaling, is a target of the  $\beta$ -catenin/TCF pathway. *Oncogene*. 2004; 23: 8520. <https://doi.org/10.1038/sj.onc.1207892> PMID: 15378020
38. Clevers H. The cancer stem cell: premises, promises and challenges. *Nat Med*. 2011; 17: 313–9. <https://doi.org/10.1038/nm.2304> PMID: 21386835
39. Jardé T, Evans RJ, McQuillan KL, Parry L, Feng GJ, Alvares B, et al. In vivo and in vitro models for the therapeutic targeting of Wnt signaling using a Tet- $\Delta$ N89 $\beta$ -catenin system. *Oncogene*. 2013; 32: 883–93. <https://doi.org/10.1038/onc.2012.103> PMID: 22469981
40. Sato T, Vries RG, Snippert HJ, van de Wetering M, Barker N, Stange DE, et al. Single Lgr5 stem cells build crypt-villus structures in vitro without a mesenchymal niche. *Nature*. 2009; 459: 262–5. <https://doi.org/10.1038/nature07935> PMID: 19329995
41. Thalheim T, Quaas M, Herberg M, Braumann UD, Kerner C, Loeffler M, et al. Linking stem cell function and growth pattern of intestinal organoids. *Dev Biol*. 2018; 433: 254–61. <https://doi.org/10.1016/j.ydbio.2017.10.013> PMID: 29198564
42. Caie PD, Walls RE, Ingleston-Orme A, Daya S, Houslay T, Eagle R, et al. High-Content Phenotypic Profiling of Drug Response Signatures across Distinct Cancer Cells. *Molecular Cancer Therapeutics*. 2010; 9: 1913–26. <https://doi.org/10.1158/1535-7163.MCT-09-1148> PMID: 20530715
43. Zhong Y, Katavolos P, Nguyen T, Lau T, Boggs J, Sambrone A, et al. Tankyrase Inhibition Causes Reversible Intestinal Toxicity in Mice with a Therapeutic Index < 1. *Toxicol Pathol*. 2016; 44: 267–78. <https://doi.org/10.1177/0192623315621192> PMID: 26692561